Volume 17 | Number 5 | 7 March 2017 | Pages 741–964

Lab on a Chip

Miniaturisation for chemistry, physics, biology, materials science and bioengineering

rsc.li/loc

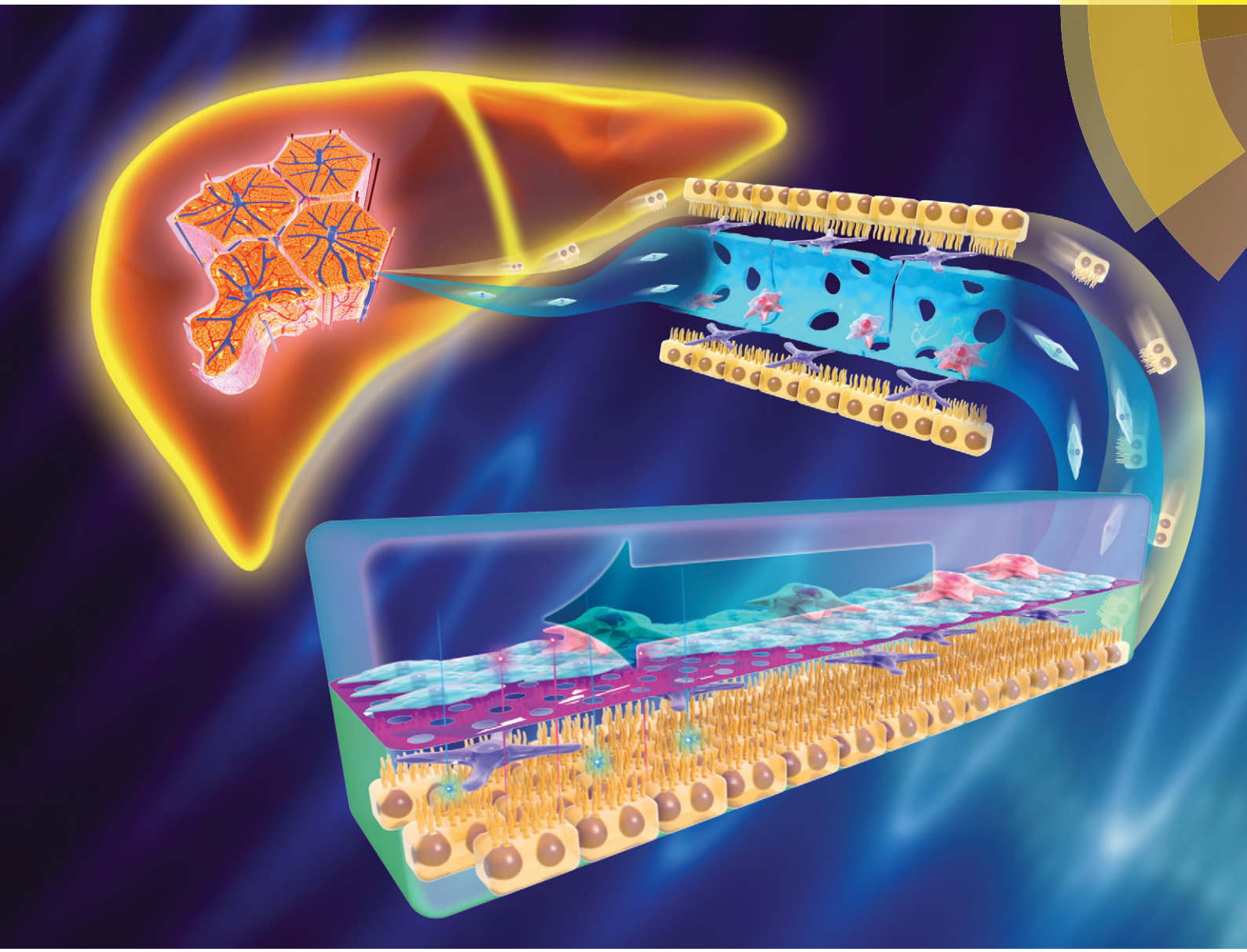

ISSN 1473-0197

ROYAL SOCIETY OF CHEMISTRY

PAPER

Mian Long *et al.*

Mimicking liver sinusoidal structures and functions using a 3D-configured microfluidic chip

Lab on a Chip

PAPER

View Article Online
View Journal | View Issue

Cite this: *Lab Chip*, 2017, **17**, 782

Mimicking liver sinusoidal structures and functions using a 3D-configured microfluidic chip†

Yu Du,[ab] Ning Li,[ab] Hao Yang,[ab] Chunhua Luo,[ab] Yixin Gong,[ab] Chunfang Tong,[ab] Yuxin Gao,[ab] Shouqin Lü[ab] and Mian Long*[ab]

Received 5th November 2016,
Accepted 12th January 2017

DOI: 10.1039/c6lc01374k

rsc.li/loc

Physiologically, four major types of hepatic cells – the liver sinusoidal endothelial cells, Kupffer cells, hepatic stellate cells, and hepatocytes – reside inside liver sinusoids and interact with flowing peripheral cells under blood flow. It is hard to mimic an *in vivo* liver sinusoid due to its complex multiple cell–cell interactions, spatiotemporal construction, and mechanical microenvironment. Here we developed an *in vitro* liver sinusoid chip by integrating the four types of primary murine hepatic cells into two adjacent fluid channels separated by a porous permeable membrane, replicating liver's key structures and configurations. Each type of cells was identified with its respective markers, and the assembled chip presented the liver-specific unique morphology of fenestration. The flow field in the liver chip was quantitatively analyzed by computational fluid dynamics simulations and particle tracking visualization tests. Intriguingly, co-culture and shear flow enhance albumin secretion independently or cooperatively, while shear flow alone enhances HGF production and CYP450 metabolism. Under lipopolysaccharide (LPS) stimulations, the hepatic cell co-culture facilitated neutrophil recruitment in the liver chip. Thus, this 3D-configured *in vitro* liver chip integrates the two key factors of shear flow and the four types of primary hepatic cells to replicate key structures, hepatic functions, and primary immune responses and provides a new *in vitro* model to investigate the short-duration hepatic cellular interactions under a microenvironment mimicking the physiology of a liver.

1. Introduction

The liver is a unique organ in the human body with a complicated structure, a sophisticated microenvironment, and multiple cell–cell interactions. A liver sinusoid, the elementary building block of the largest abdominal organ, is mainly composed of four types of cells (liver sinusoidal endothelial cells or LSECs, Kupffer cells or KCs, hepatic stellate cells or HSCs, and hepatocytes or HCs) to form two fluid channels (sinusoidal microvasculature and Disse space) within a three-dimensional (3D) microenvironment of the extracellular matrix (ECM).[1] As the sinusoidal vascular channel and Disse space are separated by a porous vascular bed consisting of flattened LSECs perforated by small fenestrae, flowing blood could penetrate through an endothelium and access the parenchymal cells.[2] Meanwhile, the organ undergoes multiple functions including dynamic metabolism, detoxification, and immune response,[3] which are hard to be specified using *in vivo* models.

In the past decades, *in vitro* two-dimensional (2D) or 3D liver models have been developed for understanding the pathophysiology, diagnosis and treatment of liver diseases, mainly applying the patterned HC culture alone or a co-culture of HCs with nonparenchymal cells (NPCs). These 2D or 3D models are likely to favor LSEC morphology and phenotype,[4–6] enhance albumin (ALB) and urea secretion,[4–17] promote cytochrome activity,[4–7,10–12] or augment bacteria susceptibility.[11] Fluid flow is another key factor to better mimic physiological environments in the sinusoid. In either microfluidic or conventional parallel flow models, shear flow seems to present distinct regulating effects, since it either fosters HC polarization and increases ALB and urea secretion[6,13–17] or yields null effects.[18] Even in those models integrating both NPC co-culture and flow exposure, diverse outcomes are still observed and, then, it is hard to elucidate the potential cooperation of the two factors.[6,10,15,17–20] Moreover, distinct types of cells from different species (*i.e.*, human or mouse) or identities (*i.e.*, LSECs or embryonic fibroblasts) are often mixed in a single *in vitro* model, which bias the intrinsic responses among hepatic cells, diverge the contributions of the co-culture or

[a] *Key Laboratory of Microgravity (National Microgravity Laboratory), Center of Biomechanics and Bioengineering, and Beijing Key Laboratory of Engineered Construction and Mechanobiology, Institute of Mechanics, Chinese Academy of Sciences, Beijing 100190, China. E-mail: mlong@imech.ac.cn; Fax: +86 10 8254 4131; Tel: +86 10 8254 4131*
[b] *School of Engineering Sciences, University of Chinese Academy of Sciences, Beijing 100049, China*

† Electronic supplementary information (ESI) available. See DOI: 10.1039/c6lc01374k

blood flow applied, and bring potential side effects on their functions.

It is difficult for those traditional *in vitro* liver models to represent the complicated structure, hepatic cell composition, and mechanical microenvironments of the liver. Microfabrication techniques, such as photolithography, replicate molding, or microcontact printing, are suitable to replicate the physiological architectures, position cells and tissues, control the cell shape and function, and create 3D *in vivo* microenvironments. Recently, multiple organ-on-chip models, such as lung,[21,22] brain,[23] bone marrow[24] and intestine,[25] have been successfully built to replicate organ-level functions. Specifically, applying microfabrication techniques to an *in vitro* liver model or a liver chip is able to address those issues that traditional liver models have encountered. To date, NPC co-culture and distribution as well as fluid flow are known to regulate liver-specific functions, which call for a liver chip that integrates these multiple factors. This type of liver chip could serve as a platform for understanding the liver-specific functions in basic sciences. For example, flowing neutrophils are usually driven by blood flow into liver sinusoids and the residence of neutrophils in the sinusoids is a prerequisite for innate responses of neutrophil recruitment. This type of cell adhesion is regulated precisely by shear flow and affected by neighboring cells through physical contact or paracrine signaling pathways. Using a well-designed liver chip, these issues are readily addressed to isolate the distinct contributions of shear flow and NPC co-culture in a physiologically-mimicking structure and configuration from the same cell sources.

Here we developed an *in vitro* 3D liver chip composed of the four types of primary hepatic cells under shear flow, attempting to mimic the liver microenvironment with a well organized cell composition and quantified physical interactions. A co-culture of murine primary HCs, LSECs, KCs, and HSCs into two fluid channels that are separated by a porous membrane in a microfluidic chip replicates the liver's physiological cell composition, microscopic architecture, and mechanical microenvironment. The flow field in the liver chip was determined by computational fluid dynamics (CFD) simulations and particle tracking visualization (PTV) tests. Liver-specific functions, such as protein secretion, cytokine production, metabolism and immune responses, were analyzed.

2. Materials and methods

2.1 Microfabrication of the microfluidic liver chip

The microfluidic chip was fabricated with PDMS (Dow Corning, MI) by mixing a silicone elastomer base and a curing agent completely in a weight ratio of 9 : 1 (base : curing agent). The PDMS mixture was poured onto a silicon-wafer SU-8 template (Capital Bio Corporation, China), degassed with a vacuum desiccator (Yilibotong Company, China), and then fully cured in an oven at 85 °C for 1 h. After being carefully peeled off from the template, this PDMS gel was cut into bricks with an equal size and assembled into a 3D microfluidic chip with two flow channels. The main flowing zones of both upper and lower channels were equally sized with $H \times W \times L = 100\ \mu m \times 1\ mm \times 15\ mm$, in which two sets of inlet and outlet holes were bored for the two channels using hole punchers. A 0.4 μm-diameter pore-sized PE membrane was cut into rectangular pieces with the same brick size and optimized to cover the channel. After treating the contact surface between the upper and lower PDMS layers with a Plasma Sputtering Pump (Yilibotong, China) for 1 min, the two layers and PE membrane were aligned carefully to ensure they are fully bonded. The integrated chip was UV-sterilized for 30 min, and both the channels were coated with 100 μg ml^{-1} collagen I at 37 °C overnight before use.

2.2 Preparation of primary murine hepatic cells

Primary murine hepatic cells were isolated from 6–8 week old C57BL/6 mice (Vital River Laboratories, China). All animal experiments were approved by the Animal and Medicine Ethical Committee of the Institute of Mechanics, Chinese Academy of Sciences. A two-step collagenase digestion protocol was modified to digest liver tissues.[26,27] Briefly, the animals were anaesthetized, a 22G catheter was inserted into the portal vein, and the liver was perfused *in situ* with a Ca^{2+}-free Gey's balanced salt solution at a rate of 5 ml min^{-1} for 5 min and then switched to a collagenase IV solution at a rate of 5 ml min^{-1} for an additional 5 min. The liver was then excised, and transferred into a sterile Petri dish filled with a high glucose DMEM medium (Hyclone, UT). The organ was minced into small pieces and the collected homogenate was filtered through a cell strainer (200 μm in diameter) to remove undigested tissue fragments.

For hepatocyte isolation, the collected cell suspension was centrifuged at 54 × *g* at 4 °C for 3 min thrice, and the supernatant was discarded except for the first collection. The packed cell pellet was re-suspended in a culture medium (high glucose DMEM supplemented with 10% FBS, 100 μg ml^{-1} streptomycin and 100 U ml^{-1} penicillin) into a final concentration of 5×10^5 ml^{-1} and used immediately.

For LSEC, KC or HSC isolation, the NPC fraction was obtained from the same hepatocyte isolation perfusion. Briefly, the supernatant was centrifuged at 500 × *g* for 8 min, and the packed pellet was re-suspended with 3 ml of a 24% Optiprep solution (Axis-Shield, Norway) and loaded with 17.6% and 11.7% Optiprep solutions and 3 ml of DMEM. The cell layer between DMEM and 11.7% Optiprep, identified as primary HSCs,[27] was collected, diluted with PBS (Hyclone, UT) twice its volume, and centrifuged at 1400 × *g* for 8 min. The packed pellet was re-suspended in the culture medium into a final concentration of 1×10^6 ml^{-1} and used immediately.

The cell layer between 11.7% and 17.6% Optiprep, enriched with LSECs and KCs, was collected, diluted with PBS twice its volume, and centrifuged at 1400 × *g* for 8 min. The pellet was re-suspended in 90 μl of PBS per 10^8 cells, and

incubated with 5 μl of FITC-conjugated rat-anti-mouse CD146 monoclonal antibodies (mAbs) (MiltenyiBiotec, Germany) and 5 μl of PE-conjugated recombinant human-anti-mouse F4/80 mAbs (MiltenyiBiotec, Germany) at 4 °C in the dark for 15 min. The cells were washed twice with PBS, and re-suspended into a final concentration of 10^8 ml^{-1} for flow cytometry sorting. Using FACS Aria III (BD Biosciences, NJ), LSECs were isolated by CD146$^+$F4/80$^-$ gating, while KCs were separated by CD146$^-$F4/80$^+$ gating. After sorting, ~100% purity of LSECs and KCs was mixed in a 2 : 1 ratio as observed *in vivo*,[28] re-suspended in the culture medium into a final concentration of 5×10^6 ml^{-1}, and used immediately. Isolated HCs, LSECs, KCs or HSCs from the mouse liver were characterized by immunofluorescence staining (Fig. S1†), indicating a well-defined protocol with high quality of hepatic cells.

2.3 Set-up of the 3D liver sinusoidal liver chip

The four types of primary mouse hepatic cells were all suspended in a culture medium. 6 μl of a HSC suspension (1×10^6 ml^{-1}) was first introduced into the lower channel using a pipette tip, and the whole chip was immediately inverted after blocking the inlets and outlets of the upper channel. HSCs were then seeded and attached to the basolateral surface of a porous polyester (PE) membrane (0.4 μm in pore diameter and 10 μm in thickness) after being incubated at 37 °C in 5% CO_2 for 1 h. 6 μl of a mixed suspension (5×10^6 ml^{-1}) of LSECs and KCs was injected onto the apical surface of the upper channel, and 6 μl of HCs (5×10^5 ml^{-1}) into the bottom substrate of the lower channel. The assembled microfluidic chip was then incubated at 37 °C in 5% CO_2 for 4 h, and unattached cells were washed from both the channels after ~6 h. Medium flow was introduced to the upper channel by a PHD22/2000 syringe pump (Harvard Apparatus, MA) connected to the inlet at 0.1 or 0.5 dyn cm^{-2}. The supernatants were collected after 24 h in the presence or absence of the shear flow for the tests of protein production and secretion.

2.4 CFD analysis of the flow field in the liver chip

The flow field in the two flow channels of the liver chip was analyzed using a 2D computational model first built in realistic sizes by GAMBIT 2.0. After creating meshes and defining boundaries, the model was directly imported into FLUENT 6.3.26 software. The porous membrane was modeled using porous zone assumption. The void fraction ε was obtained from the following formula:

$$\varepsilon = \frac{\pi d^2 \rho}{4}. \quad (1)$$

Here d is the pore diameter and ρ is the pore density. As the flow in the chip could be modeled as a laminar flow through a packed bed, the pressure drop is typically proportional to the velocity and the constant inertial resistance factor can be considered to be zero. Ignoring convective acceleration and diffusion, Darcy's law is satisfied:

$$\nabla p = -\frac{\mu}{\alpha}\vec{v}. \quad (2)$$

Here p is the pressure, μ is the viscosity, α is the permeability, and v is the velocity. When modeling laminar flow through a packed bed, the Blake–Kozeny equation,[29] a semi-empirical correlation, is applicable over a wide range of Reynolds number:

$$\frac{\Delta p}{L} = \frac{150\mu}{D_p^{\,2}}\frac{(1-\varepsilon)^2}{\varepsilon}v_\infty. \quad (3)$$

Here L is the thickness of the packed bed, D_p is the mean particle diameter, and v_∞ is the velocity in the far field. Comparing eqn (2) and (3), the permeability could be identified as:

$$\alpha = \frac{D_p^{\,2}}{150}\frac{\varepsilon^3}{(1-\varepsilon)^2}. \quad (4)$$

As eqn (4) is a semi-empirical equation and it is not able to determine experimentally the porosity of the PE membrane with LSECs, we first calculated the theoretical permeability by using eqn (4) and then adjusted the permeability to 2.5×10^{-16} m^{-2} or 2.5×10^{-17} m^{-2} in the absence or presence of LSECs. These values fit well with those velocity profiles measured from PTV tests to represent the 0.4 μm porous membrane alone or together with LSECs. For a steady flow, the velocity profile within the parallel flow channel can be obtained analytically, given by a parabolic solution of the Poiseuille flow as shown in eqn (5):

$$v(y) = \frac{6\bar{v}y(h-y)}{h^2}. \quad (5)$$

Here $\bar{v}$ is the average velocity, h is the channel height, and y is the Y coordinate along the height direction. Thus, the inlet velocity profile was set as a parabolic distribution by a user defined file (UDF) to achieve faster convergence.

2.4.1 Particle tracking visualization (PTV) test. 1 μm diameter carboxylate-modified microspheres (Invitrogen, CA) labeled with orange fluorescence (540/560) were diluted with pure water to a concentration of 3.8×10^7 ml^{-1}. After adding 6 μl of the particle solution into the lower channel, its inlet and outlet were blocked. Then the particle solution was injected into the upper channel constantly at 0.1 or 0.5 dyn cm^{-2} by a syringe pump. Since the suspending particles moved together with their surrounding fluid due to the similar densities between the particle and the fluid and the small

diameter of particles themselves, the local velocity of the fluid could be calculated by tracking the movement of those fluorescent particles frame by frame. The time course of particle displacement was then analyzed using ImageJ software (National Institutes of Health, Bethesda, MD) to estimate the velocity of the particles. Particle movements were also tracked at different heights of each channel and the wall shear stress inside the two channels was determined upon the assumption that the fluid field in the parallel flow channel could be approximated to a 2D steady flow (*cf.* eqn (5)).

2.5 Neutrophil recruitment experiments

After attaching the cells on the substrates for 6 h and removing those nonadherent cells, the whole liver chip containing LSECs alone in the upper channel or four types of hepatic cells in both upper and lower channels was incubated with 1 μM LPS for 18 h. Meanwhile, murine neutrophils were isolated from bone marrow of C57BL/6 mice using a two-step Histopaque density gradient centrifugation (Sigma-Aldrich, St. Louis, MO) according to the manufacturer's instructions. Isolated neutrophils were labeled with Cell Tracker Green CMFDA (Thermo Fisher, MA) for 15 min at 37 °C to allow clear visualization inside the liver chip. After washing the channel(s) with the working medium (HBSS with calcium and magnesium, and 1% BSA), neutrophils were injected into the upper channel at a concentration of 5×10^5 ml^{-1} at a constant wall shear stress of 0.5 dyn cm^{-2} for 15 min at room temperature. Arrested neutrophils in the middle region of the upper channel were counted and then analyzed by ImageJ.

See the "Materials and methods" section in the ESI† for further information on immunostaining, confocal microscopy, ELISA, CYP activity assay, scanning electron microscopy, and statistics.

3. Results

3.1 Reconstruction of an organ-specific liver sinusoid chip

Hepatic sinusoids or the capillary beds of the liver possess a unique configuration with an endothelium consisting of flattened endothelial cells perforated by small fenestrae with a diameter of 150–200 nm and lacking basement membranes, which adjusts mass transportation between blood stream and liver tissues and permits direct or indirect interactions between blood cells and the cells underneath the sinusoidal barrier. Here a 3D *in vitro* liver sinusoid liver chip was constructed using microfluidic fabrication techniques. As illustrated in Fig. 1A, the liver chip contains two adjacent PDMS channels separated by a thin, porous PE membrane. The two PDMS layers were fabricated using conventional soft-lithography protocols, aligned carefully with a PE membrane, and then bonded permanently by an oxygen plasma treatment. The resulting microfluidic liver chip was pre-coated with collagen I on the PDMS substrate and on both sides of the PE membrane before the four types of hepatic cells are seeded. An LSEC monolayer with sparsely distributed KCs and HSCs on either side of the PE membrane was integrated with an HC monolayer immobilized on the PDMS substrate (Fig. 1B), replicating an *in vivo* configuration of those distinct cells residing in a liver sinusoid. Specifically, LSECs were lined onto the apical side of

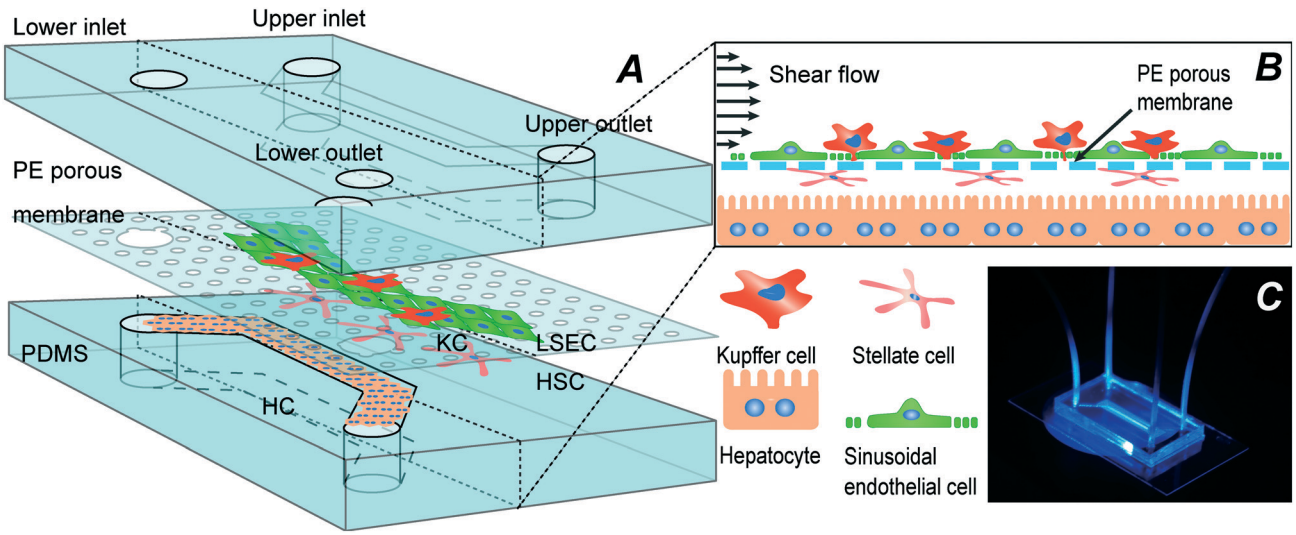

Fig. 1 Schematic of the *in vitro* 3D liver sinusoid liver chip. A. Microfluidic structure. The sinusoid liver chip is composed of two PDMS chambers of 100 μm height and 1 mm width separated by a 10 μm-thick PE membrane containing pores with 0.4 μm diameter. The upper and lower channels together with the membrane are bonded *via* plasma treatment. B. 3D assembling. The four types of hepatic cells, *i.e.* liver sinusoidal endothelial cells (LSECs), Kupffer cells (KCs), hepatic stellate cells (HSCs), and hepatocytes (HCs), are distributed layer-by-layer in a 3D manner to represent their *in vivo* feature in the hepatic sinusoid. HSCs are first injected onto the basolateral side of the collagen-I pre-coated PE membrane for sparse attachment. LSECs are then introduced onto the apical side of the membrane to form the top cell layer, followed on the top by discretely distributed KCs. HCs are placed on the collagen-I pre-coated PDMS substrate to form the bottom cell layer. All the elements are assembled together, in which the upper channel is connected to a syringe pump from one end and to a medium holder from the other end. C. Photographic image of an *in vitro* 3D liver sinusoid liver chip.

the PE membrane and KCs were then sparsely distributed (in a KC : LSEC cell number ratio of 1 : 2) on the top of LSECs, mimicking the perforated endothelial lining in an *in vivo* sinusoid. HSCs were seeded on the basolateral side of the PE membrane (also in a HSC : LSEC cell number ratio of 1 : 2), representing their *in vivo* positioning in the Disse space between sinusoidal lining cells and basal microvilli-rich HCs. Once all the cells were seeded, the upper channel was connected to a syringe pump for application of a shear stress of 0.1 or 0.5 dyn cm^{-2} on the channel substrate, reproducing their hemodynamic flow on sinusoidal lining cells exposed to the blood stream around a central vein (or zone 3 (ref. 1)). Such integration of the four major types of residing hepatic cells, all obtained from the same source of mouse liver, into two fluid channels is able to replicate those key features of a physiological sinusoid, such as the cell composition, architectural structure, and hemodynamic microenvironment (Fig. 1C).

3.2 Biological identification of hepatic cells inside the liver chip

To characterize the features of these hepatic cells in the 3D liver sinusoid liver chip, the type-specific morphology and biomarker of the four cell types were first tested in conventional dishes. It was found that these specific features were well presented and maintained, that is, glycogen-containing HCs display a polygonal shape with a double nucleus and clear edges, CD146-identified LSECs form a monolayer presenting a cobblestone shape, F4/80-identified KCs yield a polymorphic shape, and GFAP-specific HSCs present a stellate-like shape (Fig. S1†). These distinct cells were further tested after being transferred into the liver chip, *i.e.*, for HCs stained by anti-E-cadherin and anti-CK pan, LSECs by anti-CD146, and Kupffer cells by anti-F4/80 mAbs, HSCs with Cell Tracker Green, and all the cell nuclei with Hoechst 33342

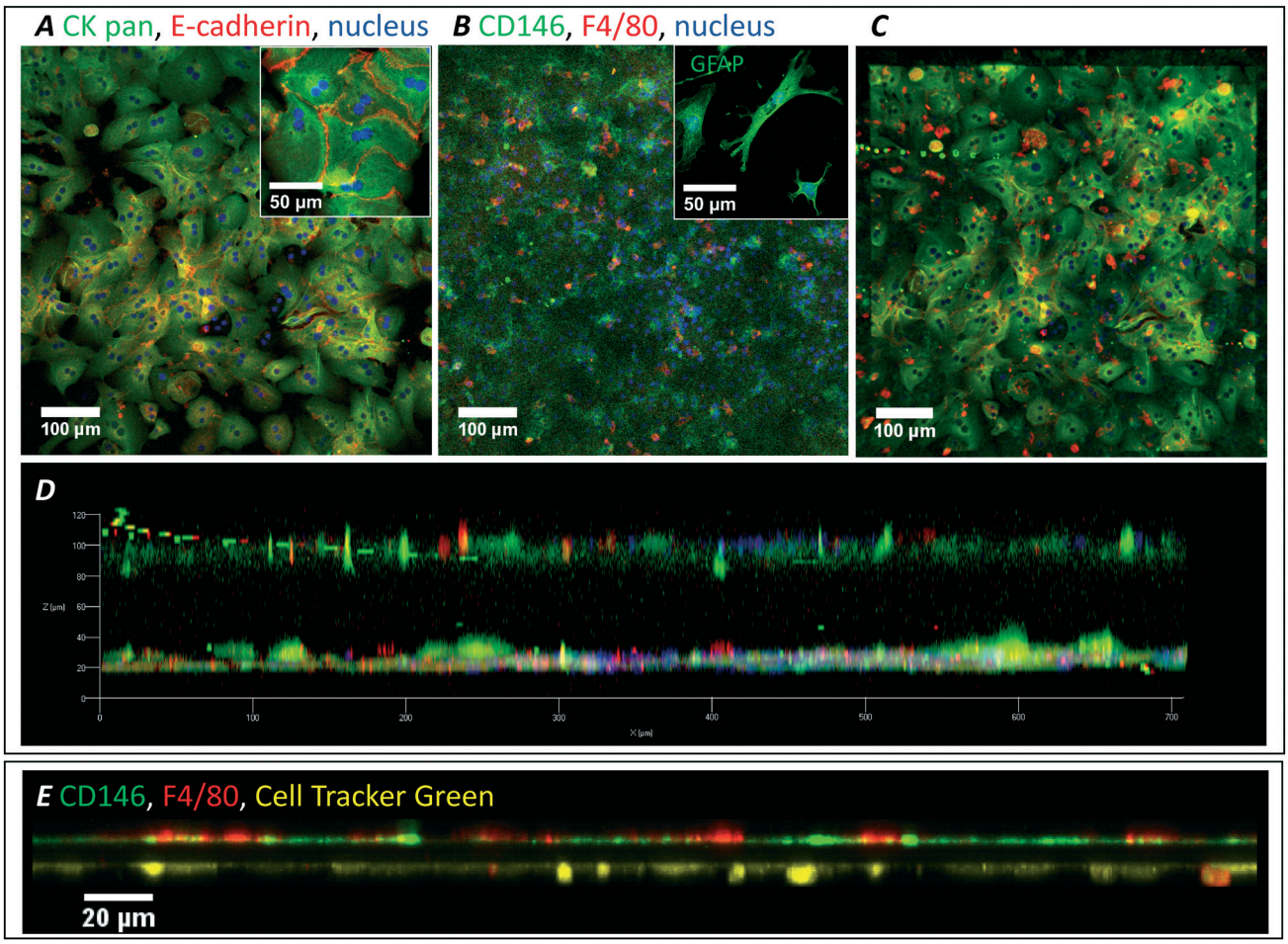

Fig. 2 Identification of the four types of mouse hepatic cells in an *in vitro* 3D liver sinusoid liver chip cultured for 1 day. A–D. Immunostaining of respective biomarkers for the distinct types of cells. Hepatocytes stained with E-cadherin (red), CK pan (green) and nucleus (blue) are closely seeded in the lower channel of the assembled liver chip. Also shown in the insert is a typical high-magnification image (A). LSECs (green; stained with CD146), KCs (red; stained with F4/80) and HSCs (unstained for clarity) are visualized together with the nucleus (blue; stained with Hoechst) in the upper channel of the assembled model. HSCs are stained with GFAP separately (green) and are present in the insert (B). Top (C) and side view (D) images of the assembled liver chip illustrate multi-types of cells in the two separated channels. E. High-magnification lateral view of a sinusoidal endothelium. LSECs (green; stained with CD146) and KCs (red; stained with F4/80) seeded on the apical side of a 10 μm-thick porous membrane, and HSCs (yellow; stained with Cell Tracker Green) placed on the basolateral side.

(Fig. 2). Within the upper channel, LSECs formed a monolayer on the apical side of the PE membrane, together with KCs sparsely anchored on top of the endothelium-like sentinels (Fig. 2B). Within the lower channel, HSCs were scattered on the basolateral side of the PE membrane (Fig. 2B) and HCs formed an intact monolayer on the channel substrate (Fig. 2A). Here HCs presented the double nuclei in one cell and were lined by continuous junctional complexes as stained by E-cadherin (insert in Fig. 2A) while HSCs were stellate-like shaped with branched structures like astrocytes (insert in Fig. 2B). The two channels were integrated well *via* visualizing the chip from the top (Fig. 2C) or side view (Fig. 2D), which clearly demonstrated the sinusoidal endothelium and parenchymal plate. A zoomed image around the PE membrane indicated that the upper LSEC layer with sparsely distributed KCs and the lower HSC layer were well separated by 10 μm-distance of the membrane height (Fig. 2E).

One of the most key features of a hepatic sinusoid is that the specified ultrastructures of LSECs are maintained, especially when attempting to build an *in vitro* liver chip. It is well accepted that the fenestrations serve as the undisputed hallmark of LSECs and the ultrastructural imaging is still the only reliable modality that allows critical evaluation. Here we examined the SEM images of LSECs cultured for 1 day on collagen I-coated glass and in the liver chip. After 1 day of culture, LSECs on the glass tended to form a relatively sparse monolayer with the sinusoidal gaps of ~1–5 μm in size on each cell body (Fig. 3A), and were perforated by small fenestrae of ~100–200 nm in size (Fig. 3B). Here the gap size found on the glass is far larger than those present *in vivo* (which yields ~400 nm^2). In contrast, LSECs in the liver chip were more flattened with sparsely distributed round holes penetrating through both the cell body and the PE membrane (Fig. 3C). Interestingly, these holes were located right on top of the pores of the porous PE membrane and yielded a similar size to those sinusoidal gaps *in vivo*. Meanwhile, LSECs were full of fenestrae with a diameter of ~100–200 nm (Fig. 3D), which are also similar to those LSEC fenestrae. Thus, the reconstructed LSEC monolayer in the liver chip was able to replicate an *in vivo* liver sinusoidal endothelium with well characterized fenestrae and sinusoidal gaps, and the LSECs were able to remain undifferentiated in the liver chip, at least, within 1 day.

3.3 Biomechanical analysis of fluid dynamics inside the liver chip

To better understand and quantify the fluid flow in the liver chip, a CFD simulation was conducted upon a model constructed upon the realistic chip geometry (Fig. 4A). Numerical calculations indicated that the flow is steady and the

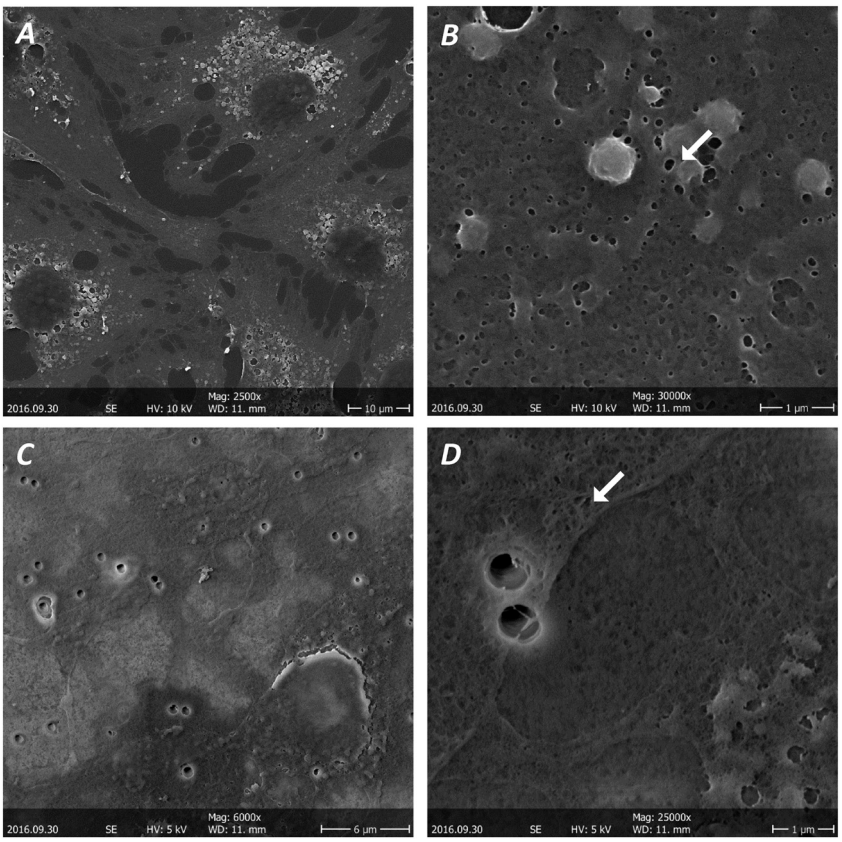

Fig. 3 LSEC identification with scanning electron microscopy. A and B. LSECs cultured for 1 day on glass at low (2500×; A) or high (30 000×; B) magnification. C and D. LSECs cultured alone for 1 day on the PE membrane in the liver chip at low (6000×; A) or high (25 000×; B) magnification. Arrows indicate those fenestrae on the cell body for both cases.

fluid velocity in the upper channel is much larger than that in the lower channel, presenting a parabolic profile at least in the upper channel (Fig. 4B). Streamlines in the upper channel are parallel to the channel substrate, coming from the inlet and terminating at the outlet (Fig. 4C). In contrast, the fluid flow in the lower channel is driven by the flow deriving from the upper channel and across the porous PE membrane, resulting in the streamlines coming from the inlet of and terminating at the outlet of the upper channel symmetrically (Fig. 4C). These data also demonstrated that the fluid is

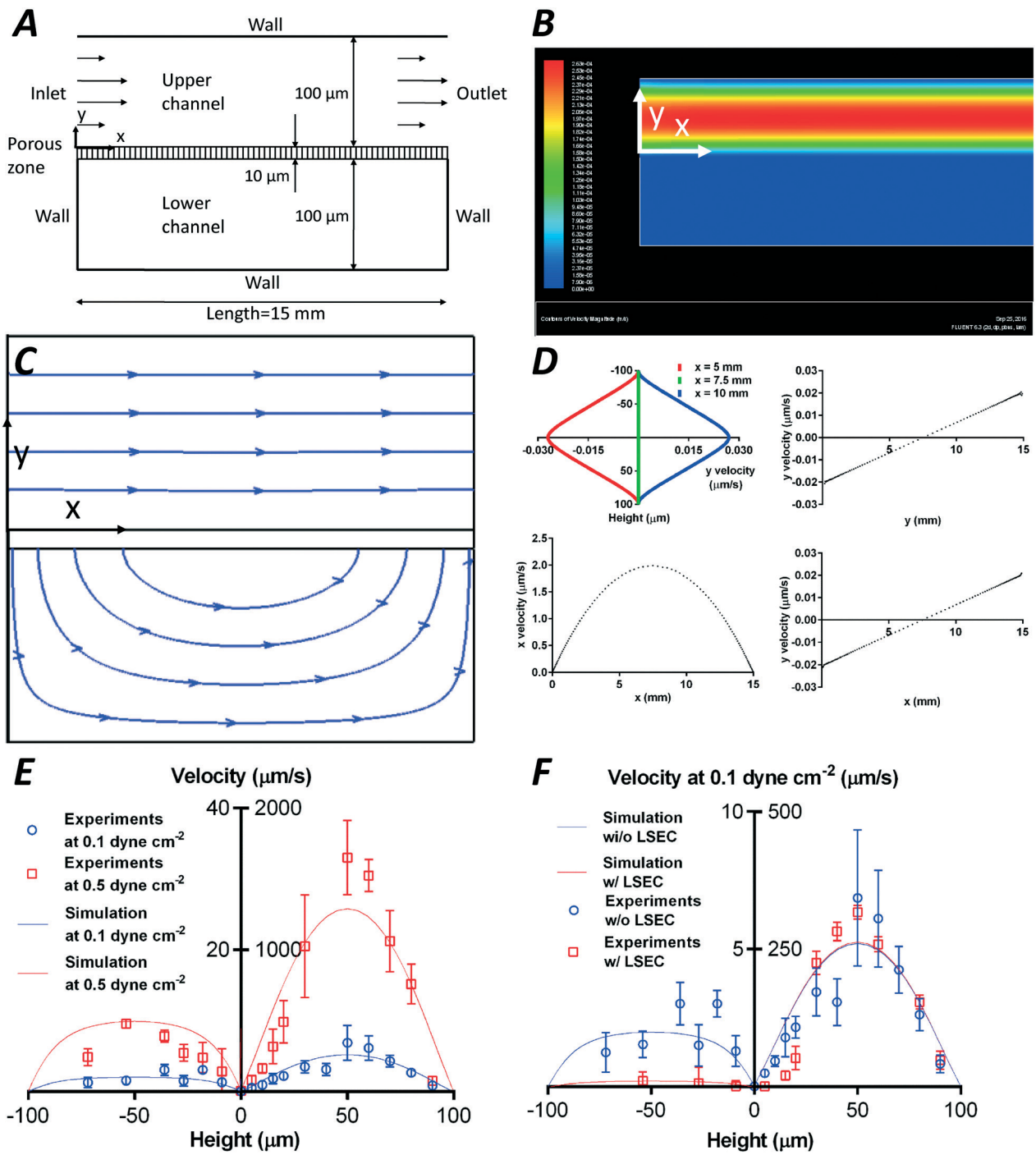

Fig. 4 CFD simulations and PTV tests of fluid flow in the liver chip. A. Geometry of the computational model (not proportional to the actual size). B. Velocity profile at the left end of the chip. C. Stream lines inside the chip. D. The *Y*-direction velocity across the chip at different positions (*X* = 5 (red), 7.5 (green) and 10 (blue) mm, upper left panel) or along the chip at 50 μm above the porous membrane (upper right panel). The *X*-Direction (down left panel) or *Y*-direction (down right panel) velocity along the chip at 50 μm below the membrane. E and F. Computational (lines) and experimental (points) *X*-direction velocity profiles at the midpoint of the liver chip (*X* = 7.5 mm), either at a wall shear stress of 0.1 (blue) or 0.5 (red) dyn cm^{-2} without LSECs (E) or in the presence (red) or absence (blue) of LSECs at 0.1 dyn cm^{-2}.

able to penetrate through the porous membrane down to the lower channel near the inlet region and pass through the membrane back to the upper channel around the outlet region. Thus, the *X*- or *Y*-direction velocity along or perpendicular to the flow direction was also calculated to characterize the flow field. Here all the *Y* velocities at different *X* positions yield negative values near the inlet region but positive ones around the outlet region in a vertically symmetric pattern (Fig. 4D, upper left panel), implying that the percolating flow is faster when the fluid is close to the porous membrane. And the *Y* velocity at a given height of $Y = +50$ μm above the membrane was found to be linear along the chip (Fig. 4D, upper right panel), indicating the percolating flow is faster at the two ends. At a given height of $Y = -50$ μm below the membrane, the *X* velocity along the chip is parabolic (Fig. 4D, lower left panel) while the *Y* velocity along the chip follows a similar linear pattern to that in the upper channel (Fig. 4D, lower right panel). These analyses provided a clue for the flow field inside the chip, which is critical for understanding mass transfer under fluid flow.

Next, we conducted PTV tests for the flow field and compared the data with the above simulations. Since the permeable flow along the *Y* direction is too slow to measure (Fig. 4D), we choose to measure the *X* velocity in the chip by visualizing the movement of suspending particles at the midpoint of the chip ($X = 7.5$ mm). In the absence of LSECs, the data presented a higher velocity profile at 0.5 dyn cm^{-2} than that at 0.1 dyn cm^{-2}, both of which all presented a parabolic distribution in either the upper or lower channel and also fitted well with the predictions from CFD simulations (Fig. 4E). In the presence of LSECs at a given shear stress of 0.1 dyn cm^{-2}, it was indicated from both the PTV tests and CFD simulations that the parabolic flow inside the chip was able to be maintained with a highly reduced magnitude of the flow velocity in the lower channel. For example, the maximal velocity in the lower channel was decreased from 2 to 0.2 μm s^{-1} (Fig. 4F), which was mainly attributed to the shielding effect of LSECs on the fluid flow. In fact, the presence of LSECs on the porous membrane blocked a large fraction of membrane pores (Fig. 3), leading to a remarkable decrease of membrane permeability.

3.4 Liver-specific secretion and cytokine cross-talk

Next, we tested ALB and urea secretion from HCs with or without fluid flow and in the presence or absence of a NPC co-culture (Fig. 5A and B). Compared with those under static conditions, the ALB secretion increased 78% for HCs alone or enhanced 50% for HCs co-cultured with NPCs at a shear flow of 0.1 dyn cm^{-2}. The combination of a NPC co-culture with flow exposure yielded even higher ALB secretion (increased 112% or 19% from HCs alone under static conditions ($P = 0.001$) or under shear flow), implying the possible cooperative effects of the two factors (Fig. 5A). These results indicated that both co-culture with NPCs and exposure of shear flow enhanced ALB secretion independently or cooperatively.

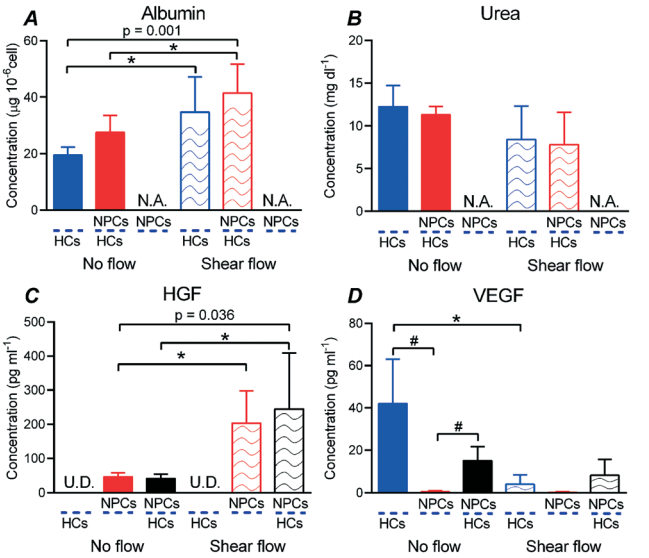

Fig. 5 Functional tests of liver-specific secretion and production from primary mouse hepatic cells with (open bars with waves) or without (solid bars) shear flow in an *in vitro* 3D sinusoid liver chip. Albumin ($n = 6$) (A) and urea ($n = 4$) (B) secretion, as well as HGF ($n = 4$) (C) and VEGF ($n = 4$) (D) production is determined from the supernatant collected at 24 h after hepatic cells are soundly attached to the substrate. The medium flows through the upper channel to exert a shear stress of 0.1 dyn cm^{-2} on the upper side of the PE membrane with or without NPCs. Plotted are the mean ± SD and statistical analysis was conducted by one-way ANOVA or *t*-test (Mann–Whitney test if the normality test failed). *, #: $P < 0.05$.

In contrast, urea secretion remained similar since no exogenous ammonia was added, no matter whether HCs were co-cultured with NPCs and/or exposed to shear flow (Fig. 5B). No significant difference was found in urea secretion, even though a descending transition was exhibited from HCs alone to HCs co-cultured with NPCs and exposed to shear flow.

HCs interact with NPCs *via* the paracrine pathway of cytokine production and present cross talk between the two cell layers. On one hand, HGF is one of the key factors secreted by NPCs (as shown in Fig. S2,† which is mainly from HSCs and partially from LSECs but not from KCs and HCs[30]) and the co-existence of NPCs may regulate the functions of HCs. Here we examined HGF production using the 3D liver chip. HCs alone do not produce HGF with or without flow, as expected. Shear flow significantly enhanced NPC-derived HGF production to 332% or 484% in the absence or presence of HCs, respectively. Intriguingly, compared with NPCs alone without flow, the combination of shear flow with an HC co-culture presented higher increase of HGF production (421%; $P = 0.036$) than the enhancement with flow for NPCs alone (332%), implying the complementary role of HCs in HGF production (Fig. 5C). Moreover, these data presented similar correlations for shear flow and cell co-culture for ALB secretion (Fig. 5A), suggesting that the increase of NPC-derived HGF production under shear flow could enhance HC-derived ALB secretion. On the other hand, the co-existence of HCs may also affect the functions of NPCs. We tested this possibility by measuring a typical VEGF cytokine

produced by HCs. Again, NPCs alone produced little VEGF with or without flow, since VEGF is mainly produced by HCs, but not by NPCs.[30] Shear flow reduced VEGF production in the absence of NPCs but restored to a similar level in the presence of NPCs. In contrast, the NPC co-culture seemed to lower VEGF production without flow but retained the same with flow (Fig. 5D). These findings are presumably attributed to less sufficient mass transportation on HCs and higher diffusive resistance in the presence of an NPC layer, compared to those HCs exposed to shear flow in the absence of an NPC layer. No further reduction was found when HCs are co-cultured with NPCs under shear flow, excluding possible cooperation of the two factors for VEGF production.

3.5 Liver-specific metabolism

Another key function of liver sinusoids is to maintain metabolic balance for the human body. CYP450 acts as the most striking cytochrome for cytotoxic metabolism in HCs and thus serves as a mature indicator. Here we tested the activities of two typical members of this family, CYP1A2 and CYP2D6, using the liver chip. Shear flow dramatically enhanced CYP1A2 (Fig. 6A) and 2D6 (Fig. 6B) activities by 530% and 628% when HCs were cultured alone or by 242% and 651% when co-cultured with NPCs, after HCs were pretreated with phenacetin and dextromethorphan, respectively. In contrast, the co-culture with NPCs had no effects on CYP activities under either static or flow conditions. Moreover, combining flow exposure with the NPC co-culture presented a remarkable increase of either CYP1A2 (277%; $P = 0.004$) or 2D6 activity (523%; $P = 0.002$). These values were slightly lower than those under shear flow in the absence of NPCs, presumably attributed to mechanical shielding of NPC layers to flow-enhanced CYP metabolism of HCs.

3.6 Hepatic cells co-culture enhanced neutrophil recruitment

Physiologically, LPS infections induce neutrophil accumulation in the liver and neutrophils tend to adhere onto and crawl along the LSEC monolayer during the recruitment (Fig. 7A). Thus, the liver chip developed here could serve as an appropriate platform to investigate hepatic cellular interactions during liver inflammation. Here we compared the accumulation of neutrophils onto LSECs alone, with KCs or together with all other three cell types of NPCs in the liver chip at a given stress of 0.5 dyn cm^{-2}. It was indicated that the number of neutrophil accumulation yielded ~138 in the field of view (FOV) for the LSECs alone, increased by 21% when co-cultured with KCs, and increased by 63% when co-cultured with all other three types of hepatic cells for 15 min of perfusion (Fig. 7B). Although KCs seemed not to contribute to liver-specific functions in terms of HGF secretion, yet their presence enhanced the accumulation of neutrophils on LSECs, possibly by increasing inflammatory cytokines secretion under stimulations.[31] And the complete replication of liver cell composition and sinusoidal configuration could further increase the accumulation of neutrophils under shear flow. During this process, most of the flowing neutrophils were not rolling over but adhered directly onto immobilized LSECs, which tended to form constantly the string-like aggregates once the first neutrophil was attached to the LSECs (Fig. 7C and D). Compared to those sparsely distributed neutrophil aggregates on LSECs alone, more and large-sized aggregates were observed on LSECs co-cultured with KCs, HSCs and HCs inside the current chip (Fig. 7D), implying that such a complete replication may also foster the formation of neutrophil aggregates.

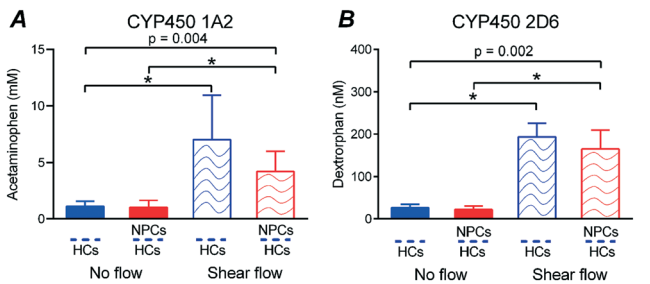

Fig. 6 Functional tests of liver-specific metabolism from primary mouse hepatic cells with (open bars with waves) or without (solid bars) shear flow in an *in vitro* 3D sinusoid liver chip. Metabolic products of phenacetin (acetaminophen, for CYP1A2 activity) ($n = 6$) (A) and dextromethorphan (dextrorphan, for CYP2D6 activity) ($n = 6$) (B) are determined by liquid chromatography-tandem mass spectrometry from the supernatant collected at 24 h at shear stress of 0.1 dyn cm^{-2}. Plotted are the mean ± SD and statistical analysis was conducted by one-way ANOVA. *: $P < 0.05$.

4. Discussion

Structural and functional similarity is challenging when replicating a living organ using an *in vitro* model, as each type of cells is indispensable to present its specific function, multiple types of cells form a 3D characterized structure in physiological anatomy, and all the cells work cooperatively in a defined mechanical or physical microenvironment with biochemical factors.[32–34] Here we developed a liver chip that integrates the four major types of hepatic cells from the same organ of origin – a murine liver – into a 3D, dual-channel microfluidic chip separated by a porous PE membrane, which allows the application of the upper channel with LSECs and KCs to mimic the sinusoidal microvasculature, the lower one with HCs and HSCs to reproduce the Disse space, and the porous PE membrane with fenestrated LSECs to replicate the sieve plate in liver sinusoids. Liver-specific functions such as protein secretion and cytokine production, drug metabolism, and neutrophil accumulation were then tested. The novelty of this work mainly lies in two aspects. First, this organ-specific liver chip presents the specified structure of an *in vivo* LSEC monolayer with the sparse gaps between neighboring cells and with the small fenestrae on individualized cells. A parabolic flow field is well formed in the two channels with different velocity magnitudes. Second, shear flow exposure and the co-culture of HC–NPC independently or cooperatively enhance the secretion of albumin, the production

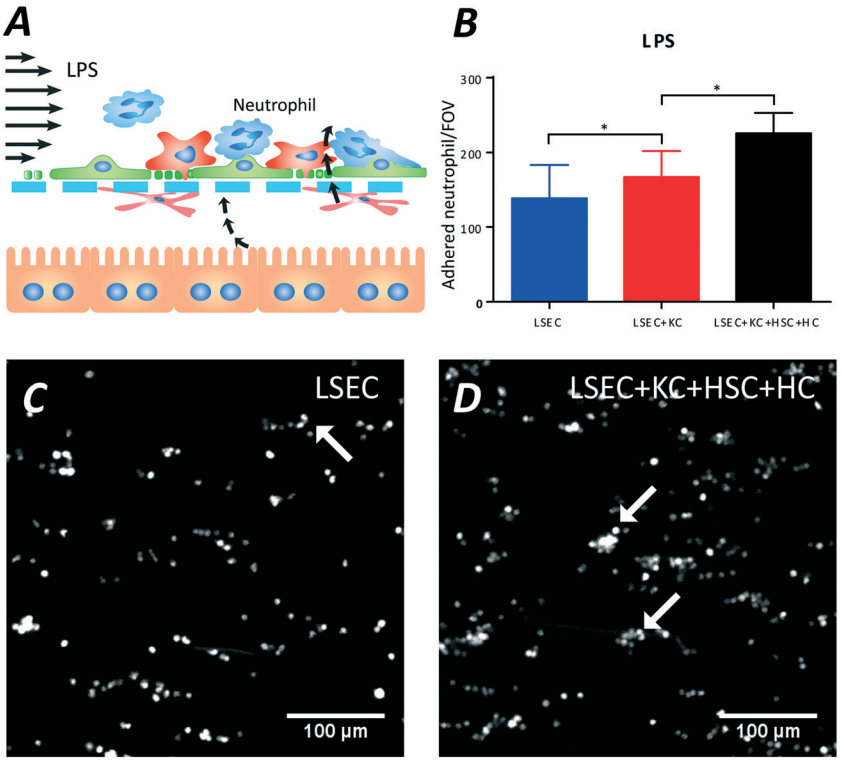

Fig. 7 Neutrophil recruitment in the liver chip under 18 h LPS stimulation. A. Schematic of neutrophil adhesion in the liver chip. B. Number of adhered neutrophils when LSECs were cultured alone, with KCs or together with the other three cell types in the liver chip. Plotted are the mean ± SD and statistical analysis was conducted by *t*-test. *: $P < 0.05$. C and D. Fluorescence-labeled neutrophils (white dots) adhere to LSECs alone (C) or co-cultured with KCs, HSCs and HCs (D) within 15 min after introducing the neutrophils into the upper channel ($n = 4$). Arrows indicated those neutrophil aggregates. Scale bar = 100 μm.

of HGF, and the metabolic activity of CYP450. Meanwhile, the co-culture of LSECs with the other three types of hepatic cells also promotes neutrophil recruitment under flow. Thus, this well defined liver chip could serve as a platform not only for basic studies but also for potential drug screening under a physiologically-alike cell composition, liver sinusoidal structure, and mechanical microenvironment compared to that of a liver.

At least two typical features are observed on the cell body of LSECs. One is the fenestrae with a diameter of 100–200 nm forming the sieve plate[1] and another is the sinusoidal gaps with a diameter of 400 nm.[2] Those features are hard to be maintained especially when primary LSECs are isolated from the liver organ and present on either the coverslip or in a microfluidic chip for a long time.[1] Using the well purified LSECs, we confirmed that these cells presented their specific fenestrae not only on the glass coverslip (Fig. 3A and B) but also on the PE membrane inside the chip (Fig. 3C and D) within at least 24 h. It is also notable that the sinusoidal gaps observed in the current chip (Fig. 3C and D) are well consistent with those in the literature,[1,2] which admits the sufficient mass transfer between the sinusoidal space and the Disse space and enables the microvilli to protrude from the parenchymal cell surface. Intriguingly, these gaps of LSECs present on the porous membrane of LSECs are likely located right on top of those pores of the membrane except for the regions close to the nucleus (Fig. 3C), suggesting that the external physical microenvironment also favors the formation of additional gaps. This is critical for building an *in vitro* liver chip since the mass transfer and oxygen exchange are usually insufficient in a close-looped microfluidic liver chip.[19] We further estimated the porosity of the current liver chip to be 12.6%, which is comparable to 15.66% in zone 1 and 11.28% in zone 3 of the rat liver at 24 h after isolation.[35] While the microfluidic model of two adjacent channels is similar to and conventional in the published organ-on-a-chip devices,[21] our focus is not only on the two fluid channels but the liver-specific architecture, in which the sinusoidal vascular channel and the Disse space are separated by a fenestrated endothelium. Here we confirmed that the four types of hepatic cells used successfully replicate the fenestrated endothelium in our liver chip. This liver-specific cellular composition and architecture make this microfluidic model suitable for basic studies of liver sinusoids, at least.

Capillary blood flow in the liver sinusoid is crucial not only for mass transfer and nutrient supply inside the conventional microvasculature bed but especially for interstitial flow inside the Disse space deriving from capillary flow across the permeable endothelium. While the liver sinusoidal endothelium is estimated to experience a fluid shear stress of 0.1–0.5 dyn cm^{-2} (ref. 36 and 37) and a fluid velocity of 10–20 cm s^{-1},[38] the flow pattern and fluid velocity profile are still

unclear in either an *in vivo* or an *in vitro* model. Here we further quantified the flow field in our *in vitro* liver chip by giving two typical physiological stresses of 0.1 or 0.5 dyn cm^{-2} as one of the initial conditions and analyzing the flow dynamics in the two channels mimicking the capillary vasculature and the Disse space, respectively. CFD simulations and PTV tests indicated that the majority of the fluid flows along the capillary-like channel and displays a parabolic flow pattern (Fig. 4B, E and F). The peak velocity at the center of the channel yields ~0.3 cm s^{-1} at 0.1 dyn cm^{-2} or 1.5 cm s^{-1} at 0.5 dyn cm^{-2} (Fig. 4E and F), which is consistent with those *in vivo* values of 10–20 cm s^{-1} when accounting for the differences in the channel height of 7–15 μm in the *in vivo* sinusoids and 100 μm in the *in vitro* chip. Moreover, the minority of the fluid flows through the permeable membrane at the inlet region, down to the interstitial-like channel, and then back to the capillary-like channel at the outlet region (Fig. 4C), which replicates well the *in vivo* flow pattern in the sinusoids. Physiologically, the interstitial flow comes from the portal regime of the capillary channel, goes through the Disse space, and finally returns to the capillary channel at the outlet regime. This recycling circulation guarantees the constant supply of fresh flow, the collection of waste products, and the exchange of cytokines between parenchymal cells and NPCs. Meanwhile, the pressure difference between the two channels generates the permeable flow across the fenestrated capillary bed, which also approximates to a parabolic pattern (Fig. 4E and F). The flow velocity in the interstitial-like channel is much lower due to the flow resistance of the fenestrated endothelium, yielding a peak value of ~2 μm s^{-1} at 0.1 dyn cm^{-2} or 10 μm s^{-1} at 0.5 dyn cm^{-2} in the absence of LSECs (Fig. 4E) or of ~0.1 μm s^{-1} at 0.1 dyn cm^{-2} in the presence of LSECs (Fig. 4F). These data are comparable with those *in vivo* values of 0.1–2 μm s^{-1},[38] which is biologically relevant since the low flow could reduce the mechanical damage to the parenchymal cells. While it is difficult to gauge the exact level of shear stress experienced by hepatocytes,[39] it has been estimated to be several orders of magnitude lower than the level of sinusoidal shear stress. As predicted by those models of interstitial flow in soft tissues, the shear stress in the Disse space could be of 10^{-6}–10^{-5} dyn cm^{-2} (ref. 37 and 40) Here we also estimated the wall shear stress in the interstitial-like channel, which yields the comparable values of 1×10^{-4}–5×10^{-3} dyn cm^{-2}. Thus, the liver chip developed here presents the well defined flow field which qualitatively mimics the *in vivo* capillary and interstitial flow in both the sinusoids and the Disse space. Furthermore, the proposed flow pattern and fluid velocity profile provide the bases in quantifying the mass transfer and nutrient supply inside the liver sinusoids.

Functional similarity is critical for replicating an *in vivo* liver sinusoid using an *in vitro* model. One key issue is the pattern of the cell co-culture. It is known that a co-culture of HCs with supporting cells promotes HC functions, but the underlying mechanisms on how multiple regulating factors work together remain unclear. For example, the 2D co-culture of a micropatterned HC monolayer or HC spheroid with embryonic fibroblasts and/or hepatic endothelial cells is able to enhance ALB and urea secretion,[5,11] but it seems hard to optimize these artificial co-cultures that are less similar to *in vivo* liver architecture. A 3D co-culture is more physiologically-like, no matter if HCs enwrap HSCs into mixed spheroids with physical contact[7] or are co-cultured with HSCs,[41] hepatic endothelial cells[31] or embryonic fibroblasts in a physically-distant manner.[5,10,17] Intriguingly, the distance between two HC and HSC layers in a physically-separated co-culture is critical for HC growth and function,[10] confirming the importance of mimicking a multiple-layered *in vivo* architecture. Here we extended this concept to develop a two-layered chip with the four major types of hepatic cells placed in a physiological configuration. HSCs in the lower channel could not contact directly LSECs in the upper channel that are separated by a 0.4 μm PE membrane, which fails to upregulate hepatocyte differentiation markers and induce ECs' capillary morphology.[41] However, these NPCs could contribute to liver-specific function through paracrine secretion (Fig. 5 and S2†). Such a co-culture pattern not only enhances ALB secretion and HGF production (Fig. 5A and C), but it is also favorable for the high metabolic activity of CYP (Fig. 6A and B). These results are consistent with the previous observations in 2D or 3D co-cultures.[10,13] Moreover, this co-culture could also enhance shear-induced neutrophil recruitment on LSECs together with NPCs (Fig. 7), presumably due to the upregulated expression and function of adhesion molecules on LSECs.[18] Thus, this proposed 3D-configured liver chip co-cultured with four types of liver cells (Fig. 1 and 2) can serve as an *in vivo*-based, accessible reference for optimizing those 2D or 3D co-cultures mentioned above, from either the architecture or function viewpoints. Meanwhile, a hybrid co-culture between hepatic cells and embryonic fibroblasts or between hepatic cells from human and mouse species may bring up extra cell- or species-based cross-talk.[4] Using autologous hepatic cells in a single *in vitro* model, if available, is recommended from our work, especially when one attempts to build structural and functional similarity with the *in vivo* liver sinusoids and identify the cell type-specific functions of each specimen systematically.

Another issue is the role of fluid flow, since multiple types of hepatic cells work together under blood or interstitial flow physiologically. Exposure of primary murine HCs to fluid flow is able to enhance ALB secretion, HGF production, and CYP activity, which is consistently found in those previous models[13–17] and our current liver chip (Fig. 5 and 6). Shear flow is also required for neutrophils to form cell strings and aggregates (Fig. 7C and D). Meanwhile, while the enhancement[6,13–17] or maintenance of LSEC phenotype (*i.e.*, SE-1 expression[25]) and function (*i.e.*, VE-cadherin, CYP3A4, AGSPR-1, ZO-1, MRP-2 expressions,[19] and leukocyte adhesion[18]) is also observed either in multiple types of cell co-cultures or under fluid flow, few studies have discussed the opposite or cooperative roles between co-culture and flow. For example, an increased flow rate is found in a perfused

human liver model using co-cultured HepRG, HUVEC, macrophages and LX-2 stellate cells, correlating with an elevated cellular oxygen consumption likely due to improved nutrient supply, but the distinct roles of cell culture and fluid flow are not isolated.[19] Here we report their synergistic enhancement of ALB secretion and HGF production and their likely opposite roles in the reduction of CYP450 metabolic activity using three different combinations of HCs–NPCs co-culture and shear flow (Fig. 5 and 6). Typically, HGF production by NPCs is enhanced when fluid flow is exerted (Fig. 5C and D), presumably due to the synergistic effect of cell co-culture and fluid flow.[30] However, CYP450 activities in HCs is decreased when NPC are co-cultured under shear flow (Fig. 6). This is presumably due to the decreased fluid flow or mass transfer delivered onto HCs in the lower channel (Fig. 4) due to the mechanical resistance of the NPC layer (Fig. 3). Meanwhile, no synergistic coordination of the two factors is observed for urea secretion and VEGF production (Fig. 5), defining the specificity of current liver chips. While the functionality of isolated primary cells and the effect of shear flow on hepatocyte function are discussed separately in the literature,[13–17] here we integrated both the factors into a single liver chip to elucidate their isolated or cooperative effects which are biologically relevant *in vivo*. It is also noticed that hepatocyte function in our liver chip can be sustained for more than 1 day, yet the LSECs' fenestrated structure disappears in 1 or 2 days after primary cell isolation found either in the literature[1] or in the current work. This chip is not specially designed for functional longevity of hepatocytes but for liver-specific functionality of liver sinusoids for short durations, as exemplified in innate immune responses in the sinusoids usually taking place within hours (Fig. 7).

Collectively, we identified the composition of primary hepatic cells and defined flow field in this liver chip and also tested the impact of cell co-culture and fluid flow on three aspects of liver-specific functions: protein secretion, cytotoxic metabolism, and immune response. Both the NPC co-culture and shear flow enhance cooperatively ALB and HGF secretion and also increase neutrophil recruitment and each type of NPCs may contribute to liver functions differently. While it is noticed that these functional tests are primary, these results provide a clue to further understand the paracrine communications and molecular mechanisms among distinct hepatic cells, especially from the viewpoint of cell–cell interactions under a mechanical microenvironment. Due to its ability to combine any types of cells, adjust spatial distributions of seeded cells, and alter the physical factors of shear flow and tissue stiffness, this liver chip could serve as a powerful platform to identify the respective roles of each type of cells and quantify the mechanical microenvironments under different physiological and pathological conditions that are not available *in vivo*.

5. Conclusion

The liver is mainly characterized by multiple types of cell co-localization under blood or interstitial flow. A 3D-configured, dynamic co-culture is prerequisite for an *in vitro* model to understand hepatic functions. Our liver chip replicates the key architecture of liver sinusoids by integrating four types of cells into two flow channels, which is able to implement liver-specific functions using primary murine hepatic cells. It also consumes a small amount of hepatic cells, is a well designed microfluidic liver chip, and is easily accessible. Thus, this new device could serve as a functional platform for understanding functional maintenance, cell–cell communication, cytotoxic metabolism, and inflammatory cascade in a liver sinusoid.

Author contributions

M. L., Y. D., N. L., and S.-Q. L. designed the study; Y. D., H. Y., C.-H. L., Y.-X. G., C.-F. T., and Y.-X. G. performed the experiments; Y. D., H. Y., and N. L. analyzed the data; and Y. D., N. L., and M. L. wrote the paper.

Competing financial interests

The authors declare neither conflict of interest nor competing financial interest.

Acknowledgements

This work was supported by the National Natural Science Foundation of China grants 31230027, 91642203, 31661143044 and 31110103918, and the CAS Strategic Priority Research Program grant XDA01030604 and XDB22040101.

References

1 B. Vollmar and M. D. Menger, *Physiol. Rev.*, 2009, **89**, 1269–1339.
2 E. Wisse, R. B. Dezanger, K. Charels, P. Vandersmissen and R. S. McCuskey, *Hepatology*, 1985, **5**, 683–692.
3 C. N. Jenne and P. Kubes, *Nat. Immunol.*, 2013, **14**, 996–1006.
4 Y. W. Liu, H. N. Li, S. L. Yan, J. J. Wei and X. H. Li, *Biomacromolecules*, 2014, **15**, 1044–1054.
5 Y. Kim and P. Rajagopalan, *PLoS One*, 2010, **5**, e15456.
6 Y. B. Kang, T. R. Sodunke, J. Lamontagne, J. Cirillo, C. Rajiv, M. J. Bouchard and M. Noh, *Biotechnol. Bioeng.*, 2015, **112**, 2571–2582.
7 S. F. Wong, D. Y. No, Y. Y. Choi, D. S. Kim, B. G. Chung and S. H. Lee, *Biomaterials*, 2011, **32**, 8087–8096.
8 H. Otsuka, K. Sasaki, S. Okimura, M. Nagamura and Y. Nakasone, *Sci. Technol. Adv. Mater.*, 2013, **14**, 5003–5013.
9 D. B. Petropolis, D. M. Faust, G. D. Jhingan and N. Guillen, *PLoS Pathog.*, 2014, **10**, e1004381.
10 S. A. Lee, D. Y. No, E. Kang, J. Ju, D. S. Kim and S. H. Lee, *Lab Chip*, 2013, **13**, 3529–3537.
11 S. March, S. Ng, S. Velmurugan, A. Galstian, J. Shan, D. J. Logan, A. E. Carpenter, D. Thomas, B. K. L. Sim, M. M. Mota, S. L. Hoffman and S. N. Bhatia, *Cell Host Microbe*, 2013, **14**, 104–115.

12 C. T. Ho, R. Z. Lin, R. J. Chen, C. K. Chin, S. E. Gong, H. Y. Chang, H. L. Peng, L. Hsu, T. R. Yew, S. F. Chang and C. H. Liu, *Lab Chip*, 2013, **13**, 3578–3587.
13 A. Dash, M. B. Simmers, T. G. Deering, D. J. Berry, R. E. Feaver, N. E. Hastings, T. L. Pruett, E. L. LeCluyse, B. R. Blackman and B. R. Wamhoff, *Am. J. Physiol.*, 2013, **304**, C1053–C1063.
14 M. Hegde, R. Jindal, A. Bhushan, S. S. Bale, W. J. McCarty, I. Golberg, O. B. Usta and M. L. Yarmush, *Lab Chip*, 2014, **14**, 2033–2039.
15 L. Prodanov, R. Jindal, S. S. Bale, M. Hegde, W. J. McCarty, I. Golberg, A. Bhushan, M. L. Yarmush and O. B. Usta, *Biotechnol. Bioeng.*, 2015, **113**, 241–246.
16 M. Jang, P. Neuzil, T. Volk, A. Manz and A. Kleber, *Biomicrofluidics*, 2015, **9**, 034113.
17 M. B. Esch, J. M. Prot, Y. I. Wang, P. Miller, J. R. Llamas-Vidales, B. A. Naughton, D. R. Applegate and M. L. Shuler, *Lab Chip*, 2015, **15**, 2269–2277.
18 S. Edwards, P. F. Lalor, G. B. Nash, G. E. Rainger and D. H. Adams, *Hepatology*, 2005, **41**, 451–459.
19 K. Rennert, S. Steinborn, M. Groger, B. Ungerbock, A. M. Jank, J. Ehgartner, S. Nietzsche, J. Dinger, M. Kiehntopf, H. Funke, F. T. Peters, A. Lupp, C. Gartner, T. Mayr, M. Bauer, O. Huber and A. S. Mosig, *Biomaterials*, 2015, **71**, 119–131.
20 E. E. Hui and S. N. Bhatia, *Proc. Natl. Acad. Sci. U. S. A.*, 2007, **104**, 5722–5726.
21 D. Huh, G. A. Hamilton and D. E. Ingber, *Science*, 2010, **328**, 1662–1668.
22 K. H. Benam, R. Villenave, C. Lucchesi, A. Varone, C. Hubeau, H. H. Lee, S. E. Alves, M. Salmon, T. C. Ferrante, J. C. Weaver, A. Bahinski, G. A. Hamilton and D. E. Ingber, *Nat. Methods*, 2016, **13**, 151–157.
23 L. M. Griep, F. Wolbers, B. de Wagenaar, P. M. ter Braak, B. B. Weksler, I. A. Romero, P. O. Couraud, I. Vermes, A. D. van der Meer and A. van den Berg, *Biomed. Microdevices*, 2013, **15**, 145–150.
24 Y. S. Torisawa, C. S. Spina, T. Mammoto, A. Mammoto, J. C. Weaver, T. Tat, J. J. Collins and D. E. Ingber, *Nat. Methods*, 2014, **11**, 663–669.
25 H. J. Kim, D. Huh, G. Hamilton and D. E. Ingber, *Lab Chip*, 2012, **12**, 2165–2174.
26 F. Braet, R. Dezanger, T. Sasaoki, M. Baekeland, P. Janssens, B. Smedsrod and E. Wisse, *Lab. Invest.*, 1994, **70**, 944–952.
27 W. Liu, Y. F. Hou, H. H. Chen, H. D. Wei, W. R. Lin, J. C. Li, M. Zhang, F. C. He and Y. Jiang, *Proteomics*, 2011, **11**, 3556–3564.
28 V. Racanelli and B. Rehermann, *Hepatology*, 2006, **43**, S54–S62.
29 S. Ergun, *Chem. Eng. Prog.*, 1952, **48**, 89–94.
30 J. J. Maher, *J. Clin. Invest.*, 1993, **91**, 2244–2252.
31 S. S. Bale, S. Geerts, R. Jindal and M. L. Yarmush, *Sci. Rep.*, 2016, **6**, 25329.
32 Z. Li, Y. Gong, S. Sun, Y. Du, D. Lü, X. Liu and M. Long, *Biomaterials*, 2013, **34**, 7616–7625.
33 D. Lü, C. Luo, C. Zhang, Z. Li and M. Long, *Biomaterials*, 2014, **35**, 3945–3955.
34 J. Wang, D. Lü, D. Mao and M. Long, *Protein Cell*, 2014, **5**, 518–531.
35 K. E. Wack, M. A. Ross, V. Zegarra, L. R. Sysko, S. C. Watkins and D. B. Stolz, *Hepatology*, 2001, **33**, 363–378.
36 P. F. Lalor and D. H. Adams, *Mol. Pathol.*, 1999, **52**, 214–219.
37 H. Rashidi, S. Alhaque, D. Szkolnicka, O. Flint and D. C. Hay, *Arch. Toxicol.*, 2016, **90**, 1757–1761.
38 O. V. Semenova, V. A. Petrov, T. N. Gerasimenko, A. V. Aleksandrova, O. A. Burmistrova, A. A. Khutornenko, A. I. Osipyants, A. A. Poloznikov and D. A. Sakharov, *Bull. Exp. Biol. Med.*, 2016, **161**, 425–429.
39 E. L. LeCluyse, R. P. Witek, M. E. Andersen and M. J. Powers, *Crit. Rev. Toxicol.*, 2012, **42**, 501–548.
40 B. Vinci, C. Duret, S. Klieber, S. Gerbal-Chaloin, A. Sa-Cunha, S. Laporte, B. Suc, P. Maurel, A. Ahluwalia and M. Daujat-Chavanieu, *J. Biotechnol.*, 2011, **6**, 554–564.
41 J. Kasuya, R. Sudo, T. Mitaka, M. Ikeda and K. Tanishita, *Tissue Eng., Part A*, 2012, **18**, 1045–1056.

